On the modeling of visco-thermal dissipations in heterogeneous porous media

Fabien Chevillotte,[a] Luc Jaouen, and François-Xavier Bécot
Matelys-Research Lab, Bât. B, 7 rue des maraîchers, F69120 Vaulx-en-Velin, France

(Received 3 April 2015; revised 2 November 2015; accepted 30 November 2015; published online 24 December 2015)

Based on a modified equivalent fluid model, the present work proposes a composite model which analytically includes the shape of the inclusions, whether they are porous or not. This model enables to describe the acoustic behavior of a large range of media from perforated plates to arbitrarily shaped porous composites including configurations of porous inclusions in solid matrix or double porosity media. In addition, possible permeability interactions between the substrate material and the inclusions are accounted for. © *2015 Acoustical Society of America*.
[http://dx.doi.org/10.1121/1.4937773]

[KVH] Pages: 3922–3929

I. INTRODUCTION

The acoustical modeling of porous media has been the subject of numerous studies for some decades. In 1949 Zwikker and Kosten introduced the hypothesis of decoupling between visco-thermal and thermal dissipation effects.[1] A few years later (1956), Biot introduced a model to take into account the elastic effect in addition to the potential visco-thermal effects.[2,3] From these seminal works, refined models for visco-thermal dissipations and reformulations of Biot equations have been developed since the 1990s. Considering long wavelength compared to the characteristic size of the pores, the acoustic propagation and the dissipation through a rigid porous media may be represented macroscopically by an equivalent fluid. Semi-phenomelogical models have been widely used since the 1990s for modeling this equivalent fluid (see, for examples, Refs. 4–7).

The models above are not valid when heterogeneities have dimensions of the same order of magnitude as the acoustic wavelength. Therefore, other models were derived in order to modelize perforated plates,[8] double porosity media,[9] porous composites made of porous inclusions in a substrate porous media,[10] or, more recently, parallel assembly of transfer matrices.[11]

Considering a modified equivalent fluid model, this work suggests a new composite model which analytically includes the shape of the inclusions whether they are porous or not. This model enables one to describe the acoustic behavior of any kind of composite media from perforated plates to arbitrarily shaped porous composites including configurations of porous inclusions in solid matrices or double porosity media.

Another originality of this work is to use a weighting function for activating the pressure diffusion and the flow distortion based on the permeability contrast of the considered media.

The present work focuses on visco-thermal dissipation. According to Biot's theory, the elastic effect and their coupling with the visco-thermal dissipations can be taken into account.[14] As far as input parameters are concerned, the elastic properties of the porous composite may be evaluated using homogenization approaches.[15]

First, the principle of the semi-phenomelogical models and some derived models are briefly recalled. Then, the principle of the new model is introduced and finally comparisons with the finite element method (FEM) are presented.

II. REVIEW OF EXISTING MODELS

A. Acoustical modeling of porous media

Using semi-phenomelogical models, the visco-thermal dissipation of acoustical energy through porous media is taken into account from two complex frequency-dependent functions [the dynamic density $\hat{\rho}_{\mathrm{eq}}(\omega)$ and the dynamic bulk modulus $\tilde{K}_{\mathrm{eq}}(\omega)$], which are analytically derived from macroscopic parameters. Acoustic wavelengths are considered larger than the characteristic size of the pores. The decoupling between visco-inertial and thermal effects is also assumed to be valid.

The most popular semi-phenomenological models are the Johnson–Champoux–Allard (JCA) and the Johnson–Champoux–Allard–Lafarge (JCAL) models. Johnson *et al.*[5] derived the visco-inertial effects from macroscopic parameters. Similarly, Champoux and Allard[6] derived the thermal effects. Lafarge *et al.*[7] improved the thermal response. A synthesis of JCA and JCAL models can be found in Ref. 4. Equations of the JCAL model are written as follows.

For visco-inertial effects

$$\tilde{\rho}_{\mathrm{eq}}(\omega) = \frac{\rho_0 \alpha_\infty}{\phi}\left[1 - j\frac{\omega_v}{\omega}\tilde{G}(\omega)\right], \tag{1}$$

$$\tilde{G}(\omega) = \sqrt{1 + \frac{1}{2}jM\frac{\omega}{\omega_v}}, \tag{2}$$

with

[a]Electronic mail: fabien.chevillotte@matelys.com

$$M = \frac{8k_0\alpha_\infty}{\phi\Lambda^2}; \quad \omega_v = \frac{\nu\phi}{k_0\alpha_\infty}, \tag{3}$$

$$\nu = \frac{\eta}{\rho_0}. \tag{4}$$

For thermal effects

$$\tilde{K}_{\text{eq}}(\omega) = \frac{\gamma P_0/\phi}{\gamma - (\gamma-1)\left[1 - j\frac{\omega_t}{\omega}\tilde{G}'(\omega)\right]^{-1}}, \tag{5}$$

$$\tilde{G}'(\omega) = \sqrt{1 + \frac{1}{2}jM'\frac{\omega}{\omega_t}}, \tag{6}$$

$$M' = \frac{8k_0'}{\phi\Lambda'^2}, \quad \omega_t = \frac{\nu'\phi}{k_0'}, \tag{7}$$

$$\nu' = \frac{\kappa}{\rho_0 C_p}. \tag{8}$$

In these equations, the macroscopic parameters are ϕ, the open porosity, σ, the static airflow resistivity, Λ, the viscous characteristic length, Λ', the thermal characteristic length, α_∞, the high limit frequency of tortuosity, k'_0, the static thermal permeability, and k_0, the static viscous permeability ($= \eta/\sigma$).

For classical porous materials, the saturating fluid is air and is taken into account from its density ρ_0 and compressibility γP_0. Other parameters are the thermal conductivity κ, the heat capacity C_p, the ratio of specific heat γ, the dynamic viscosity η, and the atmospheric pressure P_0.

B. Derived models

1. Perforated plates

Atalla and Sgard suggested to model perforated plates and screens using rigid frame porous models.[8] This model is a JCA model for which the macroscopic parameters have been properly sized:

ϕ, the perforation rate,

$$\Lambda = \Lambda' = r, \tag{9}$$

$$\sigma = \frac{8\eta}{\phi r^2}, \tag{10}$$

$$\alpha_\infty = 1 + \frac{n\epsilon}{L}, \tag{11}$$

where r is the perforation radius, L is the thickness of the plate, ε is the correction length due to the flow distortion, and n is a factor depending on both upstream and downstream materials.

2. Double porosity media

Adding meso-perforations in an appropriately chosen porous medium can lead to an enhancement of the sound-absorbing performance for a given frequency range. This kind of material is called double porosity medium and is illustrated in Fig. 1. Note that the shape can be more complicated and is not necessarily circular. Olny and Boutin exposed a model for considering dissipation effects for both meso (i.e., the meso-perforations) and micro scales (i.e., the porous matrix).[9] This model can also consider the pressure diffusion effects when there is a strong permeability contrast between both scales. The resulting dynamic quantities of such a material are given by Eqs. (12) and (13),

$$\tilde{\rho}_{\text{eq}} = \frac{1}{\frac{(1-\phi_{\text{meso}})}{\tilde{\rho}_{\text{eq\_micro}}} + \frac{1}{\tilde{\rho}_{\text{eq\_meso}}}}, \tag{12}$$

$$\tilde{K}_{\text{eq}} = \frac{1}{\frac{(1-\phi_{\text{meso}})\tilde{F}_d}{\tilde{K}_{\text{eq\_micro}}} + \frac{1}{\tilde{K}_{\text{eq\_meso}}}}. \tag{13}$$

Note that ϕ_{meso} is already taken into account in $\tilde{\rho}_{\text{eq\_meso}}$ and $\tilde{K}_{\text{eq\_meso}}$ in Eqs. (12) and (13).

$\tilde{F}_d$ is the dynamic diffusion function defined by

$$\tilde{F}_d = 1 - j\frac{\omega}{\omega_d}\frac{\tilde{D}(\omega)}{D(0)}, \tag{14}$$

$$\omega_d = \frac{(1-\phi_{\text{meso}})P_0 k_{0\_\text{micro}}}{\phi_{\text{micro}}\eta D(0)}, \tag{15}$$

$$\tilde{D}(\omega) = \frac{D(0)}{j\frac{\omega}{\omega_d} + \sqrt{1 + j\frac{M_d}{2}\frac{\omega}{\omega_d}}}, \tag{16}$$

$$M_d = \frac{8D(0)}{\Lambda_d^2(1-\phi_{\text{meso}})}, \tag{17}$$

Λ_d is the diffusion characteristic length of the host shape.

3. Porous materials containing specific porous inclusions

Gourdon and Seppi suggested an extension of the double porosity model for modeling material containing specific

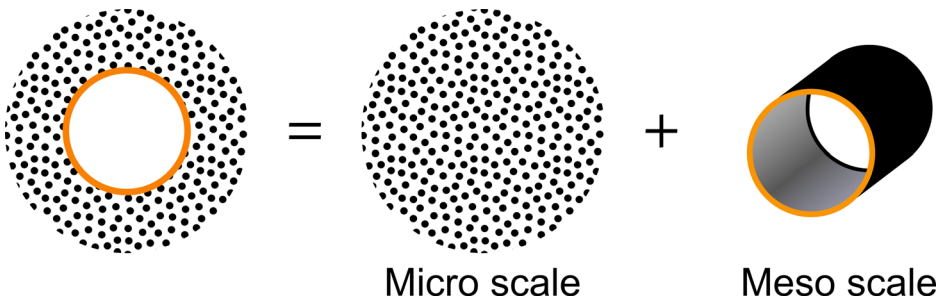

FIG. 1. (Color online) Double porosity principle. The thick line around the meso-perforation shows that the shape is taken into account.

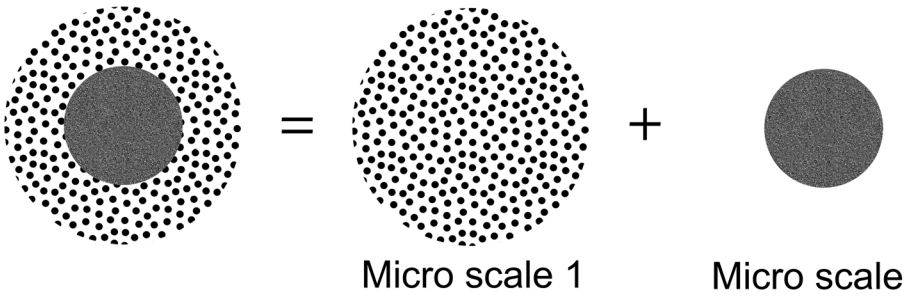

FIG. 2. Composite principle.

porous inclusions.[10] This model considers a host (H) and a client (C) material but does not account for their shape. This model is illustrated in Fig. 2. In other words, they consider a porous material that is diluted in a porous substrate. Therefore, the resulting macroscopic quantities are derived from mixing laws

$$\tilde{\rho}_{\text{eq}} = \frac{1}{\frac{(1-\phi_{\text{meso}})}{\tilde{\rho}^{H}_{\text{eq\_micro}}} + \frac{\phi_{\text{meso}}}{\tilde{\rho}^{C}_{\text{eq\_micro}}}}, \tag{18}$$

$$\tilde{K}_{\text{eq}} = \frac{1}{\frac{(1-\phi_{\text{meso}})}{\tilde{K}^{H}_{\text{eq\_micro}}} + \frac{\phi_{\text{meso}}}{\tilde{K}^{C}_{\text{eq\_micro}}}}. \tag{19}$$

Regardless of the shape of the two complementary parts, the model presented in this paper is extended to boundary cases of a typical perforated plate model and also accounts for double porosity materials.

4. Parallel assembly of transfer matrices

The transfer matrix method is commonly used in order to simulate multi-layer assembly in series. Recently, Verdière *et al*. proposed a way to assemble parallel transfer matrices.[11] This approach enables one to model interesting assemblies but considering that there is no interaction between parallel media. It implies that the diffusion effect is set aside when the two complementary media present a high permeability contrast.

III. PROPOSED COMPOSITE MODEL

Based on a modified equivalent fluid model, the principle of the proposed composite model is to analytically include the shape of the inclusions whether they are porous or not. This model enables to describe the acoustic behavior of any kind of composite media from perforated plates to arbitrarily shaped porous composites including configurations of porous inclusions in solid matrix or double porosity media as depicted Fig. 3.

A. Mesoscopic shapes modeling

Considering a shaped material with a meso-scale larger than the micro-scale of the filling porous medium (but still smaller than the macroscopic scale), it can be modeled as a semi-phenomelogical model for which the properties of the filling-fluid are modified and denoted $\tilde{\rho}_{\text{micro}}$ and $\tilde{K}_{\text{micro}}$. Equations (1), (4), (5), and (8) are replaced by Eqs. (20), (21), (22), and (23), respectively,

$$\tilde{\rho}_{\text{eq\_shape}}(\omega) = \frac{\tilde{\rho}_{\text{micro}}(\omega)\alpha_{\infty}}{\phi_{\text{shape}}}\left[1 - j\frac{\omega_v}{\omega}\tilde{G}(\omega)\right], \tag{20}$$

$$\nu = \frac{\eta}{\tilde{\rho}_{\text{micro}}(\omega)}, \tag{21}$$

$$\tilde{K}_{\text{eq\_shape}}(\omega) = \frac{\tilde{K}_{\text{micro}}(\omega)/\phi_{\text{shape}}}{\gamma - (\gamma-1)\left[1 - j\frac{\omega_t}{\omega}\tilde{G}'(\omega)\right]^{-1}}, \tag{22}$$

$$\nu' = \frac{\kappa}{\tilde{\rho}_{\text{micro}}(\omega)C_p}. \tag{23}$$

Since the shapes are complementary, the sum of mesoscopic porosities is equal to one

$$\phi^{H}_{\text{shape}} + \phi^{C}_{\text{shape}} = 1. \tag{24}$$

B. Diffusion effect modeling

The diffusion function $\tilde{F}^{i}_{d}$ is computed for each shape i (H or C). Then, a weighting function c^{i}_{w} determined for each shape allows to activate the pressure diffusion. Based on experiments and FEM simulations, the full diffusion effect is activated

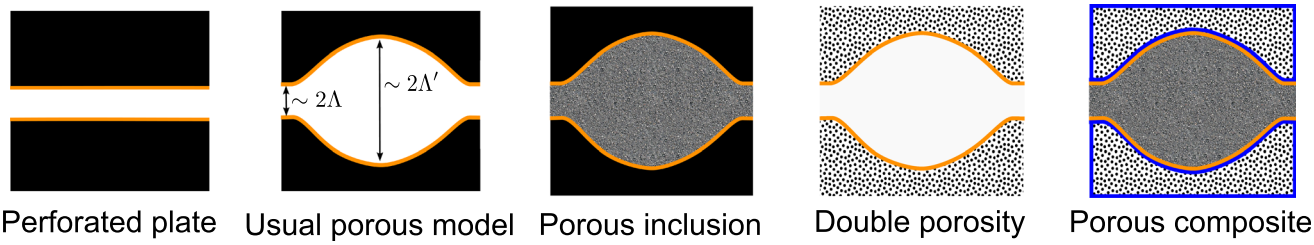

FIG. 3. (Color online) Illustration of material types taken into account from the proposed model. Parts in black represent the impervious regions. Thick lines show where the shape is taken into account.

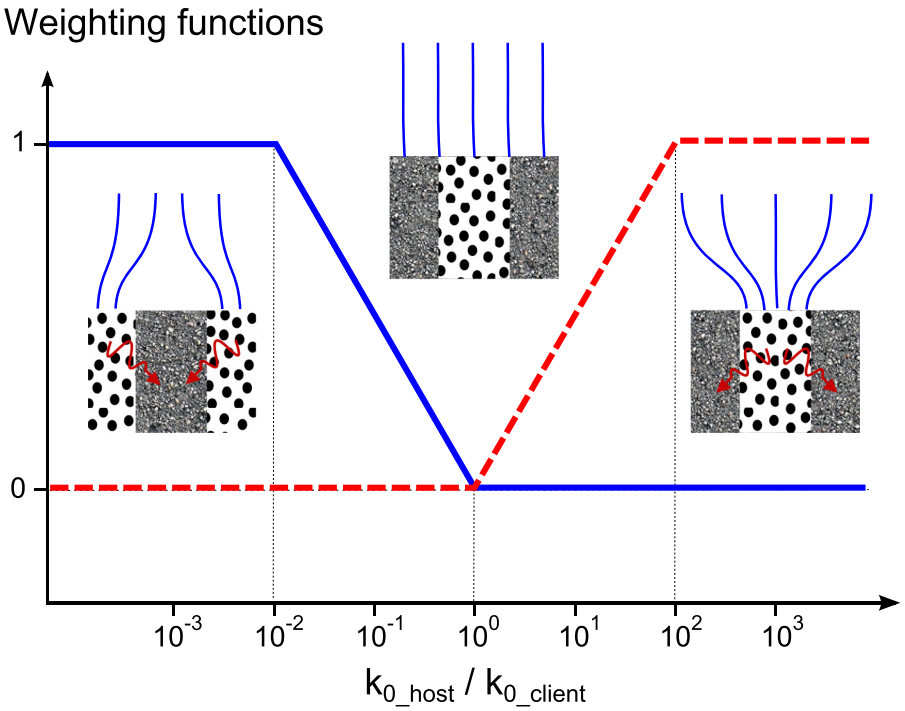

FIG. 4. (Color online) Weighting functions as a function of the permeability contrast. Weighting function of the host (solid line), weighting function of the client (dashed line).

for a permeability ratio higher than 100 (2 orders of magnitude). The pressure diffusion effect occurs from the highest permeable medium to the lowest one. The diffusion effect cannot be activated for both shapes at the same time. The weighting functions are illustrated in Fig. 4 and can be expressed as functions of the permeability contrast ξ in Table I,

$$\xi = \log_{10}\left(\frac{k_{0\_\text{host}}}{k_{0\_\text{client}}}\right). \tag{25}$$

This weighting function is the easiest to connect the behavior with and without the diffusion effect. An example of weighted diffusion function is illustrated in Fig. 5. The diffusion functions of each shape only depend on their macroscopic parameters

$$D^i(0) = k'^i_{0\_\text{shape}}, \tag{26}$$

$$\tilde{F}^i_d = 1 - j\frac{\omega}{\omega_d}\frac{\tilde{D}^i(\omega)}{k'^i_{0\_\text{shape}}}, \tag{27}$$

$$\omega^i_d = \frac{\phi^i_{\text{shape}} P_0 k^i_{0\_\text{micro}}}{\eta \phi^i_{\text{micro}} k'^i_{0\_\text{shape}}}, \tag{28}$$

$$\tilde{D}^i(\omega) = \frac{k'^i_{0\_\text{shape}}}{j\frac{\omega}{\omega^i_d} + \sqrt{1 + j\frac{M^i_d}{2}\frac{\omega}{\omega^i_d}}}, \tag{29}$$

TABLE I. Weighted functions for host c^H_w and client c^C_w depending on the permeability ratio.

if $\xi < -2$	$k_{0\_\text{client}} \gg k_{0\_\text{host}}$	$c^H_w = 1$	$c^C_w = 0$
if $-2 \leq \xi < 0$	$k_{0\_\text{client}} > k_{0\_\text{host}}$	$c^H_w = -\xi/2$	$c^C_w = 0$
if $0 \leq \xi < 2$	$k_{0\_\text{client}} \leq k_{0\_\text{host}}$	$c^H_w = 0$	$c^C_w = \xi/2$
if $\xi \geq 2$	$k_{0\_\text{client}} \ll k_{0\_\text{host}}$	$c^H_w = 0$	$c^C_w = 1$

$$M^i_d = \frac{8 k'^i_{0\_\text{shape}}}{\Lambda^{i2}_d \phi^i_{\text{shape}}}, \tag{30}$$

$\Lambda^i_d = \Lambda'^i_{\text{shape}}$ is the diffusion characteristic length of the shape i

$$\tilde{F}^i_{dw} = 1 + c^i_w[\text{Re}(\tilde{F}^i_d) - 1] + jc^i_w \text{Im}(\tilde{F}^i_d). \tag{31}$$

C. Flow distortion modeling

Models dealing with perforated plates or duct opening have to include the flow distortion effect, often called "length correction." When we deal with a composite medium made of two materials with a high permeability contrast, we should also consider this effect. An equivalent tortuosity [Eq. (11)] is calculated as suggested by Atalla and Sgard for perforated plates[8] and weighted by the weighting

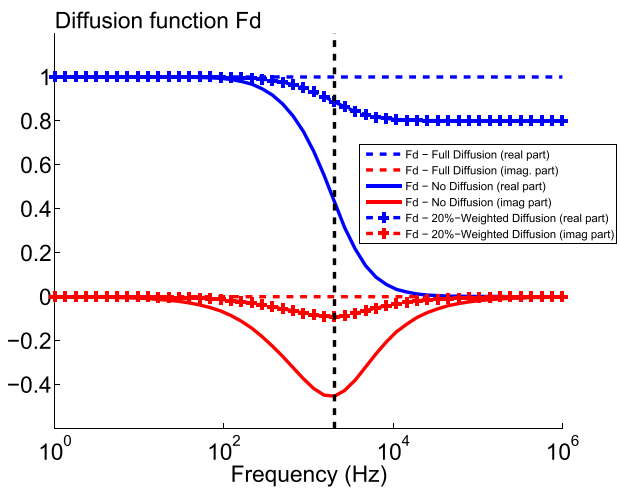

FIG. 5. (Color online) Example of weighted diffusion function for $c^i_w = 0.2$.

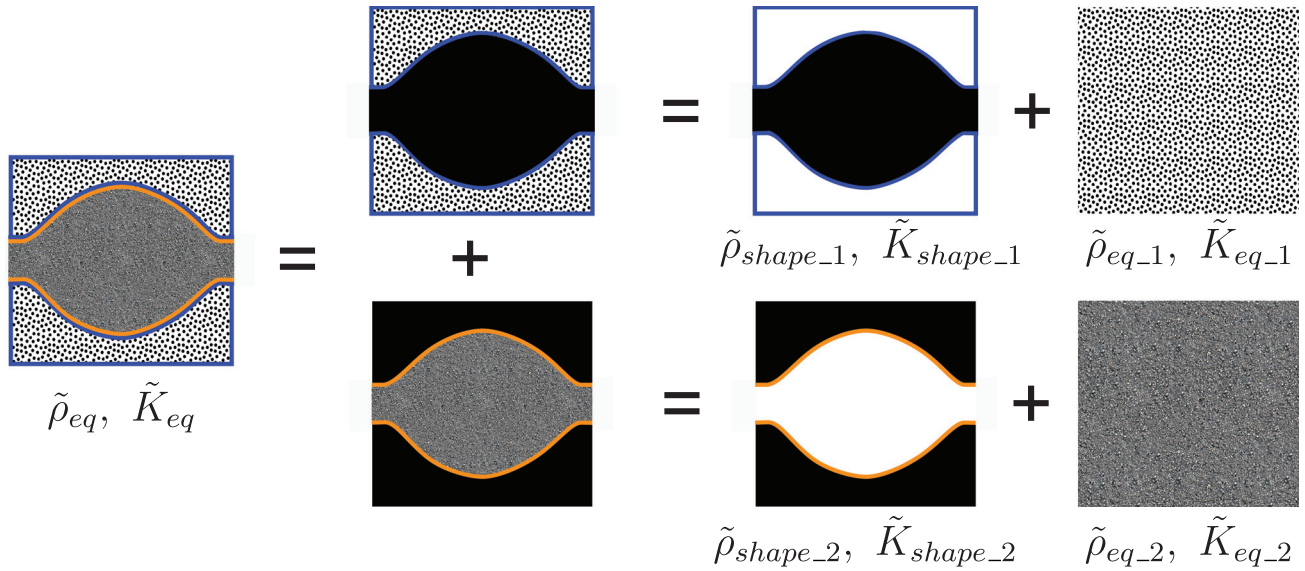

FIG. 6. (Color online) Principle of porous composite model with shape consideration.

function c_w^i for each shape. The flow distortion effect cannot be activated for both shapes at the same time. If the permeability contrast is weak, there is no flow distortion effect. If the permeability contrast is higher than 100, the full flow distortion effect is used on the highest permeable medium. Note that the model does not take into account nonlinear effects due to particle velocity amplitude within the perforations.

D. Assembly modeling

Once the properties of the host and the client are computed, the mixing law is used [Eqs. (32) and (33)]. Finally, four semi-phenomelogical models are employed to model a composite material with two complementary-shaped porous media (cf. Fig. 6)

$$\tilde{\rho}_{\mathrm{eq}} = \frac{1}{\dfrac{1}{\tilde{\rho}^{H}_{\mathrm{eq\_shape}}} + \dfrac{1}{\tilde{\rho}^{C}_{\mathrm{eq\_shape}}}}, \tag{32}$$

$$\tilde{K}_{\mathrm{eq}} = \frac{1}{\dfrac{\tilde{F}^{H}_{dw}}{\tilde{K}^{H}_{\mathrm{eq\_shape}}} + \dfrac{\tilde{F}^{C}_{dw}}{\tilde{K}^{C}_{\mathrm{eq\_shape}}}}. \tag{33}$$

$\tilde{F}^{H}_{dw}$ is the weighted diffusion function from medium C to H ($C \rightarrow H$) and $\tilde{F}^{C}_{dw}$ is the weighted diffusion function from medium H to C ($H \rightarrow C$).

TABLE II. Macroscopic parameters of materials.

Material	ϕ	σ	Λ'	Λ	α_∞	ρ	E	ν	η
Units		N s m^{-4}	μm	μm		kg m^{-3}	Pa		
Dissipative air ($d = 5$ mm)	1	23	2500	2500	1				
P1	1.00	1×10^6	12	12	1				
P2	0.96	11 500	138	108	1.01				
P3	0.98	150 000	35	30	1.00	20	500 000	0.1	0.1
P4	0.99	10 000	200	100	1.00	11	200 000	0.42	0.1

For practical implementation:

- compute the filling media properties [Eqs. (1) and (5) for porous media],
- compute the shape properties [Eqs. (20) and (22), this is not necessary if the shape is filled by a solid material],
- compute the permeability ratio ξ and the weighting functions c_w^H and c_w^C,
- compute the weighted diffusion functions $\tilde{F}^{H}_{dw}$ and $\tilde{F}^{C}_{dw}$,
- compute equivalent properties using Eqs. (32) and (33).

IV. VALIDATION EXAMPLES

In this section, a set of validation simulations is carried out and compared with FEM simulations. These latter simulations are obtained using an in-house axisymetrical model. Elements are 6-order spires. The lateral boundary conditions are sliding conditions. For each simulation, the convergence has been checked using refined meshes.

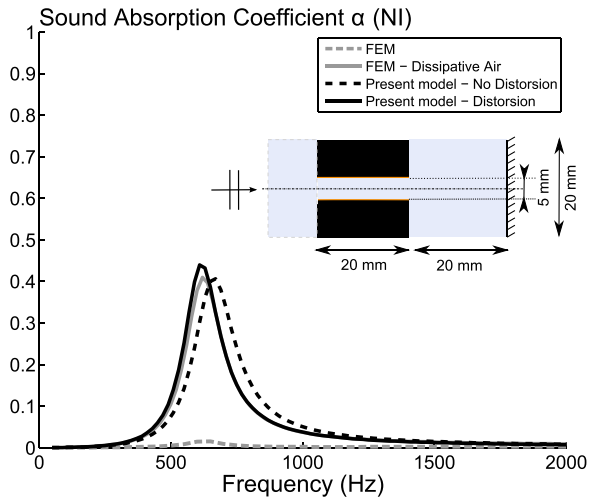

FIG. 7. (Color online) Sound absorption coefficient of perforated plate backed by an air cavity. Configuration with flow distortion. Normal incidence plane wave.

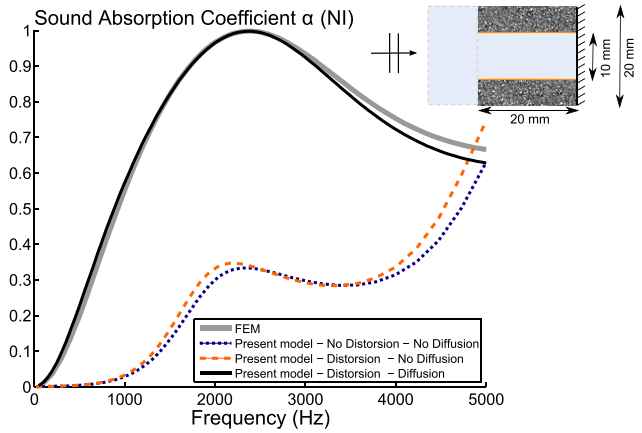

FIG. 8. (Color online) Sound absorption coefficient of double porosity media. Configuration with pressure diffusion. Normal incidence plane wave. Host medium: P1.

The parameters of used materials are summarized in Table II.

A. Perforated plate

The first example is a 20 mm-thick perforated plate backed by a 20-mm-depth cavity (Fig. 7). The perforation diameter d is 5 mm and the sample diameter is 20 mm. This example allows to validate the simple case of a perforated plate with flow distortion (length correction). In this case the host medium is a rigid solid and the client is air. The dissipation is due to the shape of the client (cylinder). While the host is solid, its shape is not needed, and there is no pressure diffusion. The client is the highest permeable medium and the permeability ratio being higher than 100, the flow distortion is activated for the client. An air layer is added in front of the sample in the FEM model in order to simulate the flow distortion. Equivalent dissipative air should be used in the FEM model to take into account the correct dissipation in the perforation. Only the perforation radius is required to compute the dissipation of a straight cylinder saturated by air. Parameters are given in Table II.

TABLE III. Macroscopic parameters of host and client shapes.

Material	ϕ	σ	Λ'	Λ	α_∞	k_0'
Units		N s m^{-4}	μm	μm		m^2
Host shape	0.68	10	4500	4000	1.81	9.27×10^{-7}
Client shape	0.32	20	4500	3000	1.41	15.84×10^{-7}

Only a slight difference around the maximum of the absorption coefficient is observed between the proposed analytical model and the FEM.

B. Rigid frame double porosity medium

A double porosity medium is used to examine the contribution of the pressure diffusion effect. A cylindrical perforation is considered in a highly resistive porous material. The response of the material is examined for a plane wave under normal incidence excitation (impedance tube conditions). In addition, the flow distortion may be taken into account as in the previous example.

Results show a good correspondence with FEM when the pressure diffusion is considered (Fig. 8). There is a strong effect of the pressure diffusion for this low permeability host media. The difference observed at high frequencies between the proposed analytical model and the FEM results is due to a non-compliance with the separation of scales. The permeability ratio being higher than 100, the pressure diffusion is fully activated for the host medium.

C. Simple rigid porous composite

A rigid composite porous medium is used to validate the pressure diffusion effect between two porous media. The original material here is the same double porosity material used in previous example. The perforation is now filled with a low resistive material P2.

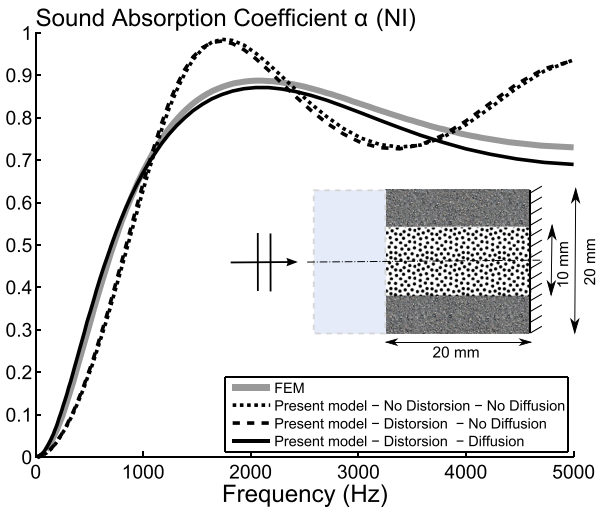

FIG. 9. (Color online) Sound absorption coefficient of composite media. Configuration with pressure diffusion between porous media. Normal incidence plane wave. Host medium: P1, Client medium: P2.

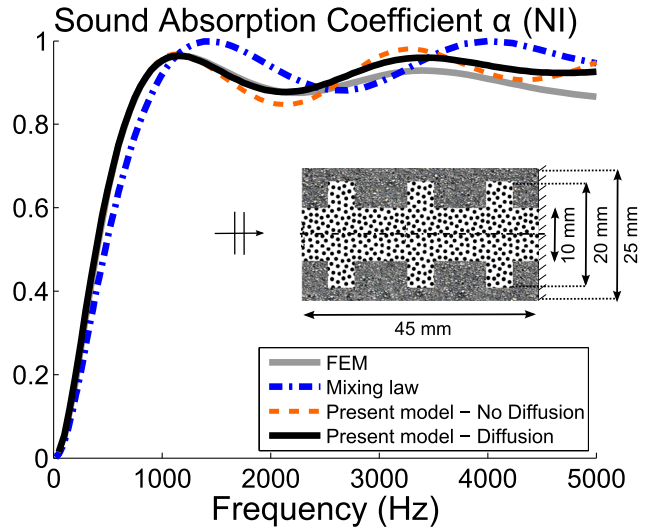

FIG. 10. (Color online) Configuration of shaped porous composite with pressure diffusion. Normal incidence plane wave. Host medium: P1, Client medium: P2.

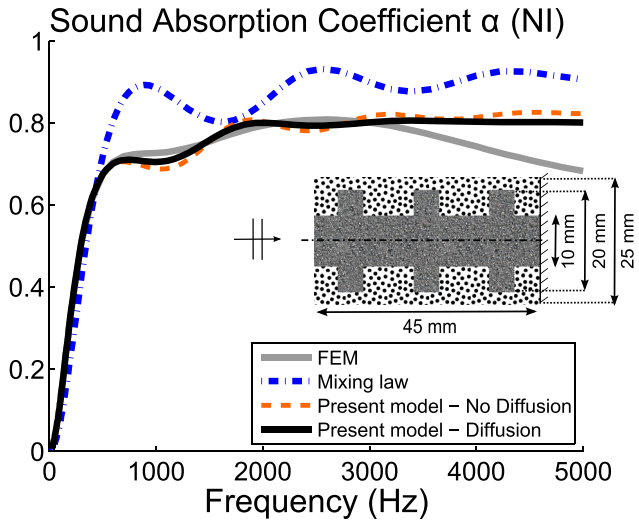

FIG. 11. (Color online) Configuration of shaped porous composite with pressure diffusion. Normal incidence plane wave. Host medium: P2, Client medium: P1.

Figure 9 shows that there is a strong effect of the pressure diffusion for this couple of porous media with a permeability contrast of 87. Once again, a good correspondence with FEM results is observed when the pressure diffusion effect is activated. As in the previous example, the difference observed at high frequencies between the proposed analytical model and the FEM results is due to a non-compliance with the separation of scales.

Note that in this case, the pressure diffusion effect tends to decrease the maximum sound absorption amplitude.

D. Tortuous rigid frame porous composite

We are now considering a tortuous mesoscopic network. The macroscopic parameters of the two shapes (host and client) are computed using the "micro–macro" approach.[12,13] These parameters are given in Table III. In this case we use

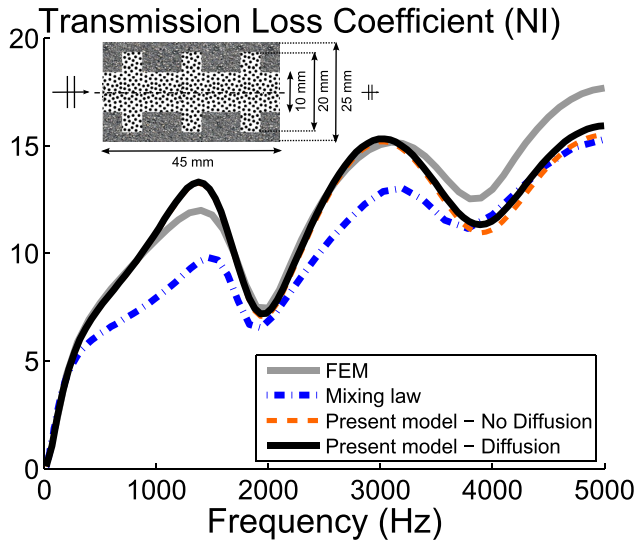

FIG. 12. (Color online) Configuration of elastic shaped porous composite with pressure diffusion. Normal incidence plane wave. Host medium: P3, Client medium: P4.

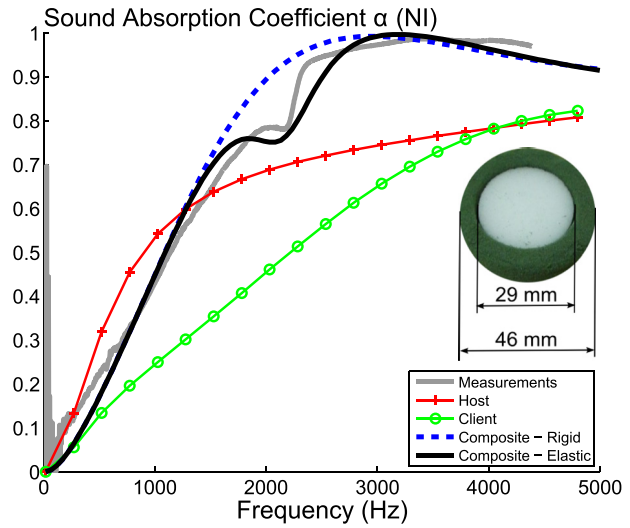

FIG. 13. (Color online) Experimental validation of elastic composite material. Normal incidence plane wave. Host medium: P3, Client medium: P4.

numerical micro–macro simulations. Nevertheless, similarly to classical porous materials, the macroscopic parameters can be obtained analytically for simple shape (circular, square, triangle, slit, etc.), numerically or experimentally. Results are given in Figs. 10 and 11. In these simulations, the mesoscopic shapes are unchanged but the filling materials have been interchanged.

A good correlation with FEM results is observed up to 3000 Hz. The upper limit of the frequency range of validity is due to non-compliance of the separation of scales. At these frequencies, the acoustic wavelength is no longer larger than the characteristic mesoscopic size (wavelength in air at 3000 Hz is around 114 mm).

In these cases, the pressure diffusion effect is lower compared to previous cases. The main observed effect is the tortuosity added by the mesoscopic shapes. Note that the pressure diffusion effect always occurs from highest permeable medium (P2) to the lowest one (P1).

E. Tortuous elastic frame porous composite

We are now investigating an example of sound transmission configuration. In this case, elastic effects have to be taken into account (Figs. 12 and 13). The Halpin-Tsai equations are used in order to forecast the equivalent elastic parameters.[15] The general equations of the Young's modulus E and the Poisson's ratio ν of a unidirectional composite material are

$$E = E^H \phi^H_{\text{shape}} + E^C \phi^C_{\text{shape}},$$
$$\nu = \nu^H \phi^H_{\text{shape}} + \nu^C \phi^C_{\text{shape}}. \tag{34}$$

In these cases, the pressure diffusion effect is negligible and the main observed effect is the tortuosity added by the mesoscopic shapes. In order to illustrate this statement, a model considering that inclusions are diluted inside the sample is also implemented (i.e., a simple mixing law). This model does not succeed in reproducing accurately the tortuous effect observed here.

Again the difference observed at frequencies higher than 3000 Hz is due to a non-compliance with the separation of scales. The differences around 1500 Hz are probably due to the approximation of the shape or the equivalent elastic parameters estimated from Eq. (34).

This example shows that this heterogeneous visco-thermal model can also be used for transmission configurations by using Biot's theory.

F. Experimental validation on a simple composite

Finally a simple 19-mm-thick composite sample is experimentally studied. The host material is a resistive material (P3) with a low resistive inclusion (P4). Measurements reveal a quarter wavelength resonance around 2200 Hz. The mesoscopic characteristic size (29 mm) is larger than the micro-scale ($\approx$100 μm). The geometry being cylindrical, the Halpin-Tsai equations are used to forecast the equivalent elastic parameters[15] and the elastic effects are coupled with the visco-thermal dissipation using Biot's theory.

The acoustic behavior of the composite medium is clearly different from the host and client ones and is reproduced by the presented model. Several limitations may explain the deviation with simulated data: the limit of the separation scale at high frequency, the equivalent elastic parameters are estimated from Eq. (34), the elastic parameters of the foams may depend on the frequency, and the boundary conditions between host and client are difficult to estimate accurately.

V. CONCLUSION

A composite model which takes into account the shapes of the heterogeneities has been presented. Its main interest is to unify the classical derived models from perforated plates to arbitrarily shaped porous composites including configurations of porous inclusions in solid matrix or double porosity media. This model allows one to consider the pressure diffusion effect and the flow distortion when client and host media have a high permeability contrast. This model has been validated with various configurations using FEM models, with or without pressure diffusion, with or without flow distortion, and with simple or tortuous shapes. Finally, it has been shown that this visco-thermal model can be used with Biot's theory in order to include elastic effects, e.g., when sound transmission properties are considered. A simple experimental validation has been presented. Future works will focus on new concepts of composite media to take full benefit of the pressure diffusion and flow distortion effects.

[1]O. C. Zwikker and C. W. Kosten, *Sound-Absorbing Materials* (Elsevier, New York, 1949), Chap. 2, 174 pp.

[2]M. A. Biot, "Theory of propagation of elastic waves in a fluid-saturated porous solid. I. Low-frequency range," J. Acoust. Soc. Am. **28**(2), 168–178 (1956).

[3]M. A. Biot, "Theory of propagation of elastic waves in a fluid-saturated porous solid. II. Higher frequency range," J. Acoust. Soc. Am. **28**(2), 179–191 (1956).

[4]J. F. Allard and N. Atalla, *Propagation of Sound in Porous Media. Modeling Sound Absorbing Materials*, 2nd ed. (Wiley, Chichester, UK, 2009), Chap. 5, 358 pp.

[5]D. L. Johnson, J. Koplik, and R. Dashen, "Theory of dynamic permeability and tortuosity in fluid-saturated porous media," J. Fluid Mech. **176**, 379–402 (1987).

[6]Y. Champoux and J. F. Allard, "Dynamic tortuosity and bulk modulus in air-saturated porous media," J. Appl. Phys. **70**, 1975–1979 (1991).

[7]D. Lafarge, P. Lemarinier, J. F. Allard, and V. Tarnow, "Dynamic compressibility of air in porous structures at audible frequencies," J. Acoust. Soc. Am. **102**, 1995–2006 (1997).

[8]N. Atalla and F. Sgard, "Modeling of perforated plates and screens using rigid frame porous models," J. Sound Vib. **303**, 195–208 (2007).

[9]X. Olny and C. Boutin, "Acoustic wave propagation in double porosity media," J. Acoust. Soc. Am. **114**, 73–89 (2003).

[10]E. Gourdon and M. Seppi, "Extension of double porosity model to porous materials containing specific porous inclusions," Acta Acoust. **96**, 275–291 (2010).

[11]K. Verdière, R. Panneton, S. Elkoun, T. Dupont, and P. Leclaire, "Transfer matrix method applied to the parallel assembly of sound absorbing materials," J. Acoust. Soc. Am. **134**(6), 4648–4658 (2013).

[12]F. Chevillotte, C. Perrot, and R. Panneton, "Microstructure based model for sound absorption predictions of perforated closed-cell metallic foams," J. Acoust. Soc. Am. **128**(4), 1766–1776 (2010).

[13]C. Perrot, F. Chevillotte, M. T. Hoang, G. Bonnet, F.-X. Bécot, L. Gautron, and A. Duval, "Microstructure, transport, and acoustic properties of open-cell foam samples: Experiments and three-dimensional numerical simulations," J. Appl. Phys. **111**, 014911 (2012).

[14]F.-X. Bécot and L. Jaouen, "An alternative Biot's formulation for dissipative porous media with skeleton deformation," J. Acoust. Soc. Am. **134**(6), 4801–4807 (2013).

[15]J. C. Halpin and J. L. Kardos, "The Halpin-Tsai equations: A review," Polym. Eng. Sci. **16**(5), 344–352 (1976).